

Stability of rotors supported in gas bearings with bushes mounted in air rings

Krzysztof Czolczyński, Tomasz Kapitaniak, Krzysztof Marynowski

Division of Dynamics, Technical University of Łódź, ul. Stefanowskiego 1/15, 90-924 Łódź, Poland

Received 20 January 1996; accepted 18 April 1996

Abstract

When during the operation of rotors supported in gas bearings their rotational velocity reaches a sufficiently high value, the loss of steady-state stability occurs. This instability is caused by the loss of damping properties of the gas film, which leads to self-excited vibrations. These vibrations are the basic obstacle to a widespread application of gas bearings.

The phenomenon of self-excited vibrations can be avoided by introducing an elastic supporting structure between the bearing bushes and the casing, characterised by properly selected stiffness and damping coefficients. In practice such a structure can have the form of an externally pressurised gas ring.

In this paper we demonstrate, on the basis of selected examples, which ranges of the values of stiffness and damping coefficients of the gas ring make it possible to retain steady-state stability at practically any rotational velocity of the rotor. We also show a design of the ring structure, especially of its feeding system, which ensures the required values of stiffness and damping coefficients (with regard to the stability). Our investigations have been carried out by means of a numerical simulation method with the use of a mathematical model of the gas bearing, verified already many times.

Keywords: Gas bearings; Stability

1. Introduction

Gas bearings in comparison with oil bearings and rolling bearings exhibit numerous indisputable advantages: they operate without noise, they have a low moment of friction, they do not generate heat and are not subjected to wear. These advantages of gas bearings are due to the fact that the surfaces of the journal and bush are separated by a gas (mainly air) layer characterised by a very low (when compared with oil) viscosity. Gas bearings retain their advantages at high rotational velocities which exceed significantly the maximum rotational velocities admissible for oil bearings and rolling bearings.

The main disadvantage of gas bearings, which prevents their widespread applications, are the self-excited vibrations occurring when a sufficiently high rotational velocity is achieved.

The phenomenon of self-excited vibrations is manifested by the fact that at a certain boundary value of the rotational velocity, the steady-state stability is lost and the bearing journal begins to move along the trajectory whose radius increases until the journal reaches its stable boundary cycle. At the same time the frequency of the self-excited vibrations is equal

to the half of the angular velocity—the so-called ‘‘half-whirl’’. When the boundary rotational velocity is exceeded even by a few per cent, the radius of the boundary cycle is bigger than the radial clearance of the bearing, and thus the phenomenon of self-excited vibrations leads fast to the journal–bush contact and, as a result, to the destruction of the bearing.

As early as in 1965 the investigations (numerical simulations) carried out by Lund showed that the boundary rotational velocity of the rotor can be increased by an introduction of a system of linear springs and viscous dampers between the bushes of the gas bearings and the casing [1]. This phenomenon was also confirmed during later laboratory experiments conducted by Kerr [2] and Kazimierski and Jarzecki [3]. Those researchers used rubber rings between the bearing bushes and the casing. Kerr’s as well as Marsh’s [4] laboratory experiments also showed that the use of rubber rings reduced the width of the region of self-excited vibrations and that there was a (theoretical) possibility of the rotor operation over the unstable region.

Czolczyński’s numerical experiments [5–7] have shown that an introduction of the isotropic system of linear springs and viscous dampers between the bearing bushes and the

casing brings about only a slight increase in the boundary rotational velocity (the success of the above-mentioned researchers should be evaluated as moderate), but it leads to a limitation of the range of rotational velocities at which self-excited vibrations occur. The main effect of his works was that he demonstrated that a proper selection of the values of stiffness and damping coefficients of the elastic bush support leads to a vanishing of the unstable regions, that is, to an elimination of the phenomenon of self-excited vibrations. Further investigations carried out by Czolczyński and Marynowski have provided data on the ranges of stiffness and damping coefficients, which make it possible to avoid the loss of the steady-state stability of symmetrical rotors supported in self-acting bearings [8] and in externally pressurised bearings [9], as well as of non-symmetrical rotors [10]. During these investigations an original method for a determination of the values of stiffness and damping coefficients of gas bearings was used [7,11]. This method can also be used for externally pressurised bearings (as opposed to the small perturbation method which can be used only for self-acting bearings [12]).

The present paper presents a practical solution of an elastic bush support of gas bearings, whose stiffness and damping coefficients fall within the required ranges (in the light of the results included in Refs. [8–10]).

What is proposed here is an external gas ring surrounding the bearing bush. This ring must be of course externally pressurised because the bearing bushes do not rotate and thus, a dynamic load carrying wedge does not occur here.

During our numerical simulations we tested several gas rings which differed in terms of the boundary conditions imposed on the gas film and in terms of the feeding system structure.

2. Rotors supported in gas bearings—our object of interest

A possibility of eliminating self-excited vibrations is shown here on the example of the rigid, symmetrical rotor supported in two gas bearings with flexibly mounted bushes (Fig. 1).

The rotor parameters are as follows:

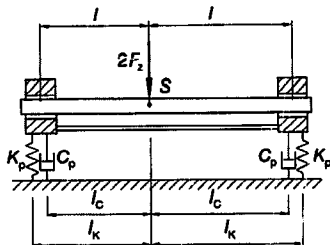


Fig. 1. Symmetrical rotor supported in two flexibly mounted gas bearings.

mass $m^* = 228.0$ kg ($m = 0.42$)
 moment of inertia $B^* = 68.7$ kg m² ($B = 42$)
 distance between the bearings $2l^* = 1.9$ m ($2l = 34.6$)
 The parameters of the bushes (joined by a common base):
 mass $m_p^* = 65.0$ kg ($m_p = 0.12$)
 moment of inertia $B_p^* = 58.8$ kg m² ($B_p = 36$)
 distance between the springs and dampers $2l_k = 2l_c = 2l$
 The parameters of the bearings:
 length $L = 0.11$ m
 radius $R_1 = 0.055$ m
 radial clearance $c_1 = 30 \times 10^{-6}$ m
 gas viscosity $\mu = 18.2 \times 10^{-6}$ kg m⁻¹ s⁻¹ (air)

We are investigating self-acting and externally pressurised bearings. The feeding system of the externally pressurised bearings consists of 16 feedholes, located in two rows in 1/4 and 3/4 of the length of the bearing. The radius of the feedhole is $r_{01} = 0.15 \times 10^{-3}$ m, and the supply pressure $p_0^* = 0.7 \times 10^6$ Pa (dimensionless supply pressure $p_0 = p_0^* / p_a = 7$).

The parameters of the bearings create the basis for the computations of dimensionless parameters of the rotor and the bush (quoted above in brackets), according to the formulae included in the Appendix. These parameters are also the basis for a determination of the relation between the dimensional and dimensionless values of stiffness and damping coefficients and of the force.

The bearings are loaded by the rotor weight $2F_z^* = 2200$ N, which means that the dimensionless loading force acting on the journal of each bearing is equal to $F_z = 3.5$. The external pressurised bearings transfer this force at the relative eccentricity $\epsilon \approx 0.35$. (The exact value of ϵ depends of course on the value of the rotational velocity.) The linearised equations of the rotor and bush motion (which are easy to be derived) are mentioned in Refs. [7–9]. In these equations, dynamical properties of the gas film are represented by four stiffness and four damping coefficients.

3. The ranges of stiffness and damping coefficients of the elastic support which allow to avoid self-excited vibrations

Fig. 2 shows the stability maps of the considered systems with externally pressurised bearings for two selected values of the stiffness coefficient of the elastic support K_p and various values of the damping coefficient C_p (on the horizontal axis). On the vertical axis, the values of the dimensionless rotational velocity Λ of the rotor are represented.

When $K_p = 22$ (thin lines), there are three regions in which self-excited vibrations occur. For $C_p < 1.1$ or $C_p > 2.5$ (on the left-hand side of the point A_{22} or on the right-hand side of the point B_{22}), at a sufficiently high rotational velocity Λ , the loss of the stability of conical modes of vibrations occurs (thin dotted lines). Irrespective of this, a continuous region of self-excited vibrations of cylindrical modes of vibrations

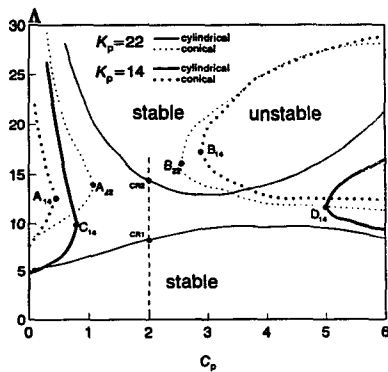


Fig. 2. Stability thresholds of the rotor supported in externally pressurized bearings; $m = 0.42$, $B = 42$, $m_p = 0.12$, $B_p = 36$, $p_0 = 7$, $F_z = 3.5$.

(thin solid lines) existing for all the values of C_p can be observed. Though all these unstable regions are limited, an attempt to exceed them may result in the destruction of the bearing.

The situation changes with the stiffness coefficient of the bush support $K_p = 14$ (thick lines). The unstable regions of the conical modes are decreased ($A_{22} \rightarrow A_{14}$ and $B_{22} \rightarrow B_{14}$, thick dotted lines), and, which is most important, the continuous unstable region of cylindrical modes is divided into two subregions—self-excited vibrations with the cylindrical modes may occur only for $C_p < 0.85$ or $C_p > 5$ (on the left-hand side of the point C_{14} or on the right-hand side of the point D_{14} , thick solid lines). It means that for $K_p = 14$ and $0.85 < C_p < 2.9$, between the points C_{14} and B_{14} there is not any unstable region and the self-excited vibrations do not occur, irrespective of the value of the rotational velocity A .

Fig. 3 exhibits the boundaries of unstable regions for cylindrical and conical modes of vibrations as the functions of the parameters C_p and K_p of the elastic bush support. The boundaries that can be seen in Fig. 2 are marked here. The region in which both cylindrical and conical modes of vibrations

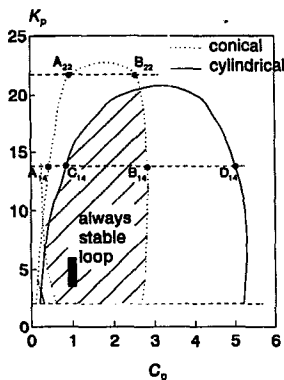


Fig. 3. Stability map and always stable loop.

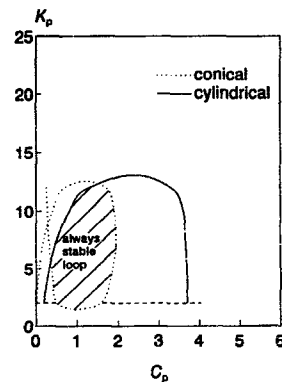


Fig. 4. Stability map and always stable loop—self-acting bearings.

remain stable irrespective of the value of the rotational velocity is hatched. This region has been called an “always stable” loop.

In Fig. 4 the analogous boundaries of unstable regions and an “always stable” loop for a rotor supported in self-acting bearings are shown. More detailed data about an influence of different parameters of the system (F_z , m , m_p , B , B_p , p_0) on the size of “always stable” loops can be found in Refs. [8–10].

4. Mathematical model of the air ring

The basis of the mathematical model of the gas ring is the Reynolds equation describing a pressure distribution in the gas film [13,14].

$$-\frac{\partial}{\partial \theta} \left(PH_1^3 \frac{\partial P}{\partial \theta} \right) - \frac{\partial}{\partial \xi} \left(PH_1^3 \frac{\partial P}{\partial \xi} \right) + \Lambda \frac{\partial}{\partial \theta} (PH_1) + \frac{\partial}{\partial \tau} (PH_1) = \frac{dn}{2C} \frac{d\theta}{d\xi} \quad (1)$$

In the model of the air ring, the gas film is divided into axial and circumferential directions. For each grid point i, j , the Reynolds equation may be written after a few transformations in the following form of finite differences:

$$\begin{aligned} & \frac{H_{1ij}}{P_{ij}} \frac{\Delta Q_{ij}}{\Delta \tau} + 2P_{ij} \frac{\Delta H_{1ij}}{\Delta \tau} + 2\Lambda P_{ij} \frac{H_{1ij+1} - H_{1ij-1}}{2\Delta \theta} + \frac{\Lambda H_{1ij}}{P_{ij}} \\ & - 3H_{1ij}^2 \frac{(H_{1ij+1} - H_{1ij-1})(Q_{ij+1} - Q_{ij-1})}{4\Delta \theta^2} \\ & + -3H_{1ij}^2 \frac{(H_{1i+1j} - H_{1i-1j})(Q_{i+1j} - Q_{i-1j})}{4\Delta \xi^2} \\ & - H_{1ij}^3 \frac{Q_{ij+1} - 2Q_{ij} + Q_{ij-1}}{\Delta \theta^2} - H_{1ij}^3 \frac{Q_{i+1j} - 2Q_{ij} + Q_{i-1j}}{\Delta \xi^2} \\ & = 2FK_2 H_{1ij} \nu_k \pi_s \pi_d \quad (2) \end{aligned}$$

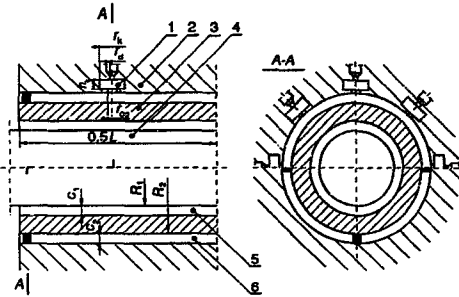


Fig. 5. Air ring with chamber feeding system: 1, chamber; 2, casing; 3, movable bush; 4, journal; 5, gas film of the bearing; 6, gas film of the air ring.

with

$$FK_2 = \frac{2\pi\sqrt{\kappa}}{\Delta\theta\Delta\xi} \beta^{(\kappa+1)/2\kappa} \left(\frac{p_0}{p_a}\right)^2 \frac{12r_{02}\mu\sqrt{\Re T_0}}{p_0 c_2^2} \quad (3)$$

The right-hand side of Eq. (2) differs from zero only for the mass source points (feedholes) i_z, j_z . To solve numerically this equation, the alternating direction implicit scheme (ADI) given in detail in Refs. [15,16] was adopted.

The way of modelling the gas flow through the chamber feeding system described below was based on the model of the so-called high stiffness bearing [17–20] and it is its simplified version.

A gas ring with a chamber feeding system is shown in Fig. 5. The gas of pressure p_0^* flows through the orifices with the cross-section area $A_d = \pi r_d^2$ to the chambers of the volume V , and then through the feedholes of the radius r_{02} to the gap between the casing and the bearing bush.

To describe the mass flow through the chamber feeding system, it is necessary to formulate:

1. A simplified relation between the mass flow through a feedhole of the radius r_{02} , and the gas film pressure distribution surrounding the feedhole.
2. A relation between a mass flow and a pressure drop for the feedhole of the cross-section $A_k = 2\pi r_{02} h_2$.
3. A relation between a mass flow and a pressure drop for the orifice of the cross-section $A_d = \pi r_d^2$.
4. Equations of continuity using relations specified above (points 1–3).

For Point 1, near a source point (i_z, j_z) the Reynolds equation may be reduced to a Laplace equation

$$\frac{\partial^2 Q_{i,jz}}{\partial \theta^2} + \frac{\partial^2 Q_{i,jz}}{\partial \xi^2} = 0 \quad (4)$$

with unknown $Q_{i,jz} = P_{i,jz}^2$ [13,21,22]. The solution of this equation in the finite difference approximation can be written in the form:

$$Q_{i,jz} = \bar{Q}_{i,jz} + \frac{\nu_k \pi_d FK_1}{H_2^2 \nu_k} \quad (5)$$

with

$$\bar{Q}_{i,jz} = \frac{(Q_{i_z-1,j_z} + Q_{i_z+1,j_z}) \frac{\Delta\theta}{\Delta\xi} + (Q_{i_z,j_z-1} + Q_{i_z,j_z+1}) \frac{\Delta\xi}{\Delta\theta}}{2 \left(\frac{\Delta\xi}{\Delta\theta} + \frac{\Delta\theta}{\Delta\xi} \right)} \quad (6)$$

$$FK_1 = \frac{r_{02} p_0}{c_2 p_a} \beta^{\frac{\kappa+148}{2\kappa}} \frac{\mu \sqrt{\kappa \Re T_0}}{p_a c_2} \frac{\frac{\Delta\xi}{\Delta\theta} \ln \left(\frac{R_2 \Delta\theta}{r_0} \right) + \frac{\Delta\theta}{\Delta\xi} \ln \left(\frac{R_2 \Delta\xi}{r_0} \right)}{2 \left(\frac{\Delta\xi}{\Delta\theta} + \frac{\Delta\theta}{\Delta\xi} \right)} \quad (7)$$

Assuming, that p_c is the pressure in the source point and using the identity

$$\pi_c = \frac{p_c}{p_1} = \frac{p_c}{p_a} \frac{1}{\pi_a} \Rightarrow \left(\frac{p_c}{p_a} \right)^2 = (\pi_a \pi_c)^2 \quad (8)$$

Eq. (5) can be written as

$$(\pi_a \pi_c \pi_0)^2 = \bar{Q} + \frac{\nu_k \pi_d FK_1}{H_2^2} \quad (9)$$

For Point 2, the real mass flow through the feedhole can be written as

$$\dot{m}_k = \nu_k \dot{m}_k^* \quad (10)$$

with the critical mass flow

$$\dot{m}_k^* = A_k p_1 \sqrt{\frac{2\kappa}{\Re T_0 (\kappa-1)}} (1 - \beta^{(\kappa-1)/\kappa}) \beta^{1/\kappa} \quad (11)$$

The coefficient $\nu_k = \nu_k(\pi_i, \beta)$ can be estimated in simplification by means of the Bendemann ellipse [21]:

$$\frac{(\pi_i - \beta)^2}{(1 - \beta)^2} + \nu_k^2 = 1 \quad (12)$$

The parameter π_i is a theoretical variable which is related to the effective pressure π_c by means of the formula

$$(1 - \pi_c) = K(1 - \pi_i) \quad (13)$$

The coefficient $K = K(\beta, \mu, c_2, h_2, p_0, \nu_k, \pi_d)$ is determined experimentally in Ref. [15] as

$$\begin{aligned} K &= 0.16 + 0.0002 \text{Re} && \text{for } \text{Re} \leq 2000 \\ K &= 0.685 + 0.155y - 0.19y^2 && \text{for } 2000 < \text{Re} < 4000, \\ &&& (y = (\text{Re} - 3000)/2000) \\ K &= 0.715 && \text{for } \text{Re} \geq 4000 \end{aligned}$$

where the Reynolds number is given by

$$\text{Re} = \beta^{(\kappa+1)/2\kappa} \frac{2\kappa}{\mu \sqrt{\kappa \Re T_0}} \nu_k \pi_d c_2 H_{2,i,jz} p_0 \quad (14)$$

Estimating π_i from Eq. (12) and π_c from Eq. (13), the equation

$$[1 - K(1 - B)(1 - \sqrt{1 - \nu_k^2})]^2 \pi_a \pi_0 = \bar{Q} + \frac{\nu_k \pi_d FK_1}{H_2^2} \quad (15)$$

can be obtained from Eq. (9), with the unknown ν_k .

For Point 3, the mass flow rate through the orifice can be calculated by means of the experimental formula [21]:

$$\nu_d = \frac{\dot{m}_d}{\dot{m}_d} = C_d \nu(\pi_d) \tag{16}$$

where

$$\dot{m}_d = A_d p_0 \sqrt{\frac{2\kappa}{(\kappa-1)\Re T_0} (1-\beta^{(\kappa-1)/\kappa}) \beta^{1/\kappa}} \tag{17}$$

$$\nu(\pi_d) = \frac{\pi_d^{1/\kappa} \sqrt{1-\pi_d^{(\kappa-1)/\kappa}}}{\beta^{1/\kappa} \sqrt{1-\beta^{(\kappa-1)/\kappa}}} \tag{18}$$

for $\beta < \pi_d \leq 1$ and

$$\nu(\pi_d) = 1 \tag{19}$$

for $\pi_d \leq \beta$.

The experimentally determined discharge coefficient $C_d = C_d(\pi_d)$ is given in Ref. [16] as $C_d = 0.85 - 0.15\pi_d - 0.1\pi_d^2$.

For Point 4, as a consequence of the bush motion, the mass flows \dot{m}_k, \dot{m}_d change with time and cause increases of the pressures p_1 in chambers:

$$\frac{p_1 - p_{10}}{\Delta t} \frac{V}{\Re T_0} = \dot{m}_d - \dot{m}_k \tag{20}$$

The subscript 0 denotes initial values of the pressure.

Substituting

$$\dot{m}_d = C_d A_d p_0 \sqrt{\frac{2\kappa}{(\kappa-1)\Re T_0} (1-\pi_d^{(\kappa-1)/\kappa}) \pi_d^{1/\kappa}} \tag{21}$$

$$\dot{m}_k = A_k p_1 \sqrt{\frac{2\kappa}{(\kappa-1)\Re T_0} (1-\pi_1^{(\kappa-1)/\kappa}) \pi_1^{1/\kappa}} \tag{22}$$

Eq. (20) may be obtained in the form

$$\nu_d A_d p_0 - \nu_k A_k p_1 = \frac{p_1 - p_{10} V}{\Delta t} FK_3 \tag{23}$$

with

$$FK_3 = \frac{1}{\Re T_0 \sqrt{\frac{2\kappa}{(\kappa-1)\Re T_0} (1-\beta^{(\kappa-1)/\kappa}) \beta^{1/\kappa}}} \tag{24}$$

Dividing Eq. (23) by p_0 gives finally the equation:

$$\nu_d A_d - \nu_k A_k \pi_d = (\pi_d - \pi_{d0}) \frac{V}{\Delta t} FK_3 \tag{25}$$

with unknown π_d (note, that ν_d is a function of π_d). The subscript 0 denotes the initial value of the pressure ratio.

Eq. (25) produces, together with Eq. (15), a system of two non-linear equations with unknowns π_d and ν_k . The solution of this system is not an easy task. It is done by the method of successive approximations.

In our investigations we also used gas rings with a direct feeding system, as those shown in Fig. 6. The mathematical model of such a ring is of course based on the Reynolds Eq. (2) and on the equations describing the relation between the mass flow through a feedhole of the radius r_{02} , the gas film

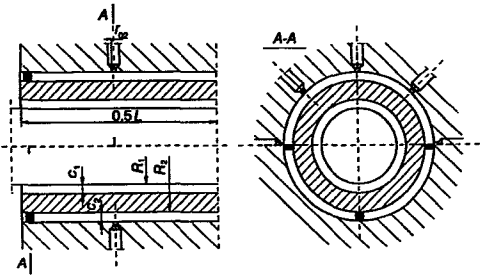


Fig. 6. Air ring with direct feeding system.

pressure distribution surrounding the feedhole, and the pressure drop for a feedhole of the cross-section $A_k = 2\pi\nu_{02}h_2$. These equations have been written above as Eqs. (4)–(15) with $p_1 = p_0$, i.e. $\pi_d = 1$.

The mathematical models of both the rings provide data on the components of the loading force in the direction of the axis x and y :

$$F_{zx} = p_d R_2^2 \int_0^{L/R_2} \int_0^{2\pi} P \cos \theta \, d\theta \, d\xi$$

$$F_{zy} = p_d R_2^2 \int_0^{L/R_2} \int_0^{2\pi} P \sin \theta \, d\theta \, d\xi \tag{26}$$

at the gap h_2 defined by the equation:

$$h_2 = c_2 (1 - \epsilon \cos(\theta - \theta_s)) \tag{27}$$

Models have been used in computing the values of stiffness and damping coefficients of gas rings by means of the method described in Refs. [7,11].

In this mathematical model of the system, the rings are represented by matrices of these coefficients. The matrices multiplied by the bush velocity components \dot{x}_p and \dot{y}_p and the bush displacement components x_p and y_p from the static equilibrium position inform us about the values of dynamic responses of the ring:

$$\begin{bmatrix} \delta F_{zx} \\ \delta F_{zy} \end{bmatrix} = \begin{bmatrix} C_{11} & C_{12} \\ C_{21} & C_{22} \end{bmatrix} \begin{bmatrix} \dot{x}_p \\ \dot{y}_p \end{bmatrix} + \begin{bmatrix} K_{11} & K_{12} \\ K_{21} & K_{22} \end{bmatrix} \begin{bmatrix} x \\ y \end{bmatrix} \tag{28}$$

It should be added, however, that during our investigations we found that the values of the coupling coefficients $C_{12}, C_{21}, K_{12}, K_{21}$ were negligibly small.

5. Externally pressurised air ring as the flexible support of the bush

5.1. Air ring with the direct feeding system

In our first investigations we made computations of the stiffness and damping coefficients of the air rings with the simplest, direct feeding system (the same as the feeding sys-

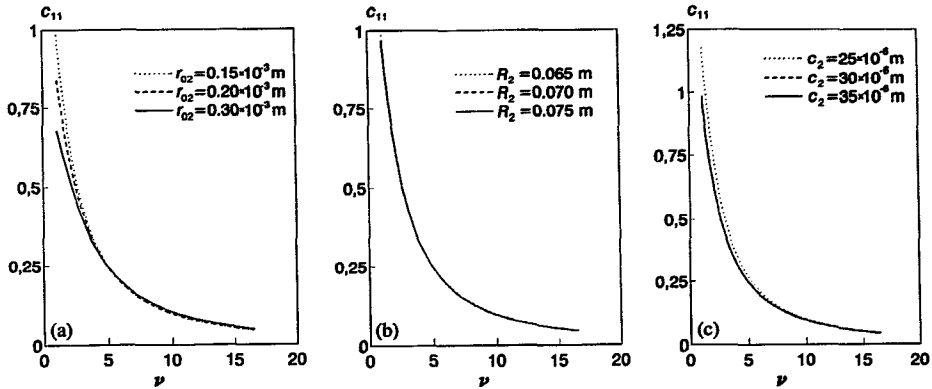


Fig. 7. Damping coefficient of air ring with direct feeding system: (a) $R_2 = 0.065$ m, $c_2 = 30 \times 10^{-6}$ m; (b) $r_{02} = 0.15 \times 10^{-3}$ m, $c_2 = 30 \times 10^{-6}$ m; (c) $R_2 = 0.065$ m, $r_{02} = 0.15 \times 10^{-3}$ m.

tem of the bearings). The length of the ring $L = 0.11$ m was equal to the length of the bearing (Fig. 6).

Figs. 7 and 8 show the values of the damping coefficient C_{11} and the stiffness coefficient K_{11} of the ring (in the plane along which the force F_z acts) for different values of the radius r_{02} of the feedholes, the ring radius R_2 and the clearance c_2 between the bush and the casing. As one can see, the changes of these basic parameters do not exert any significant influence on the value of the stiffness coefficient, or especially on that of the damping coefficient. As opposed to the arbitrarily selected constant values of the stiffness and damping coefficients K_p and C_p of the springs and dampers which support the bush shown in Fig. 1, the stiffness and damping coefficients of the gas rings depend on the frequency of vibrations ν of the bush, represented on the horizontal axes in Figs. 7 and 8. When the eccentricity ratio between the bush and the casing is small (in our examples do not exceed 0.2), the coefficients C_{22} and K_{22} (in the plane perpendicular to the plane along which the force F_z acts) are similar to C_{11}

and K_{11} . Values of the cross-coupling coefficients C_{12} , K_{12} , C_{21} and K_{21} are small in comparison with C_{11} and K_{11} . Moreover, the changes of the rotational velocity of the rotor, in the considered range of Λ , cause so small changes of the natural frequencies ν , that the air ring may be considered as the (almost) isotropic support of the bushes, like the springs K_p and dampers C_p .

As one can see, the coefficient C_{11} , which is to play a role of the coefficient C_p of the elastic bush support, has the value of magnitude of 1 only for low frequencies of vibrations. When the frequency of vibrations ν increases, this coefficient decreases rapidly. For $\nu \approx 3-4$ (self-excited vibrations of the investigated system have the frequency of this magnitude), the value of C_{11} is already smaller than 0.3. Such a damping coefficient does not ensure an elimination of self-excited vibrations—compare with the drawings of “always stable” loops (Figs. 3 and 4). The stiffness coefficient K_{11} has a value in the range 13–15. It could play a role of K_p in the case of externally pressurised bearings (Fig. 3), but only if associ-

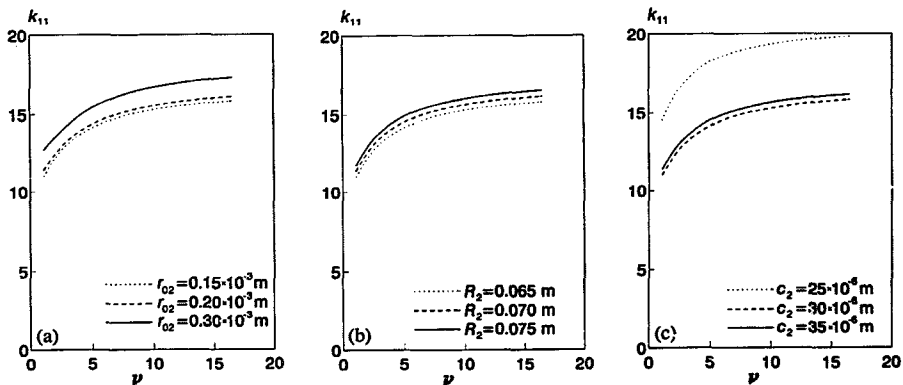


Fig. 8. Stiffness coefficient of air ring with direct feeding system: (a) $R_2 = 0.065$ m, $c_2 = 30 \times 10^{-6}$ m; (b) $r_{02} = 0.15 \times 10^{-3}$ m, $c_2 = 30 \times 10^{-6}$ m; (c) $R_2 = 0.065$ m, $r_{02} = 0.15 \times 10^{-3}$ m.

ated with the damping coefficient $C_p (= C_{11}) \approx 2$. The values of the stiffness and damping coefficients C_{22} and K_{22} of the air rings (in the plane perpendicular to the plane along which the force F_x acts) are close to C_{11} and K_{11} , and therefore their diagrams are not presented here. This remark concerns all the results presented below as well.

Aiming at an increase in the value of the damping coefficient of the gas ring, we have modified the boundary conditions of the gas film by an introduction of rubber seals at both the ends of the ring, which is shown in Fig. 9. Fig. 10(a) presents the coefficient C_{11} as a function of the frequency of vibrations of the bush for four different values of the angle γ_r (compare Fig. 9) which defines the size of the seals. The ring parameters are as follows: $L=0.11$ m, $R_2=0.065$ m, $r_{02}=0.15 \times 10^{-3}$ m, $c_2=30 \times 10^{-6}$ m. The representation of C_{11} and K_{11} corresponding to $\gamma_r=0$ (without seals) has been transposed from Figs. 7 and 8. As can be seen, the seals whose task was to hinder the air flow along the ring axis have indeed caused an increase in the values of the coefficient C_{11} . For instance, for $\nu=4$ from $C_{11}=0.29$ for $\delta_r=0$ to $C_{11}=0.67$ for $\gamma_r=2/3 \times 2\pi$. This last result would fall inside the "always stable" loop (compare Fig. 3 and Fig. 4), if not for the fact that an increase in the damping coefficient is accompanied by an increase in the stiffness coefficient K_{11} . As can be seen in Fig. 10(b), this coefficient assumes the values in the range 20–30 for $\gamma_r=2/3 \times 2\pi$, and hence above the "always stable" loop.

As a further attempt we tried to support the bearing bush in gas rings with longitudinal rubber baffles which reduce a circumferential air flow (Fig. 11). The gas film of the ring with the parameters: $L=0.11$ m, $R_2=0.065$, $r_{02}=0.15 \times 10^{-3}$ m was divided by us by means of these elastic baffles into $n_k=4, 6$ and 8 sectors. In each sector there was 1 feedhole located half way down the length of the ring. Fig. 12 presents the values of the coefficients C_{11} and K_{11} for $n_k=8$ and for three different values of the radial clearance c_2 . As can be easily seen, the values of the coefficient C_{11} again lie below the required region $C_{11} > 0.5$, and the stiffness coefficients—over the required $K_{11} < 10-15$.

Fig. 13 shows how the values of the stiffness and damping coefficients are affected by the change in the number of the sectors n_k . Our further defeat can be seen in the fact that when

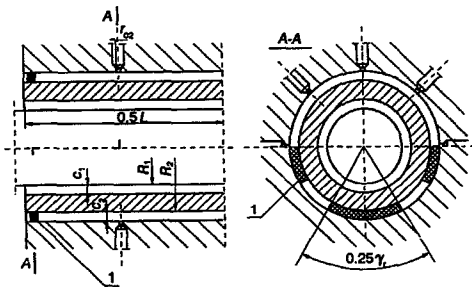


Fig. 9. Air ring with rubber seals (1).

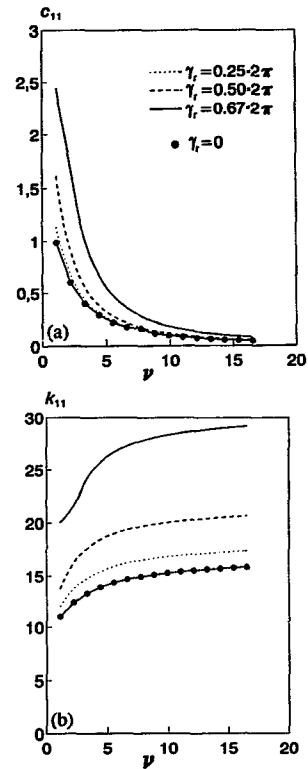


Fig. 10. (a) Damping and (b) stiffness coefficient of air ring with rubber seals.

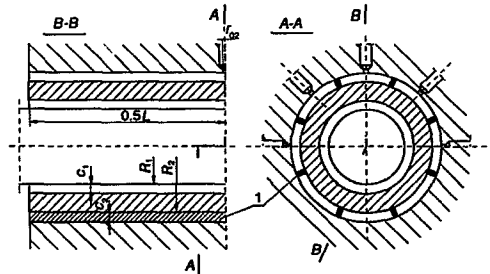


Fig. 11. Air ring with longitudinal rubber baffles (1).

for $n_k=4$ the coefficient $C_{11} \approx 0.5$ ($\nu=4$), then the coefficient K_{11} exceeds 20—we are again outside the "always stable" loop.

5.2. Air ring with the chamber feeding system

Since it has been found that the air rings with the direct feeding system do not have such stiffness and damping coefficients which ensure an elimination of self-excited vibra-

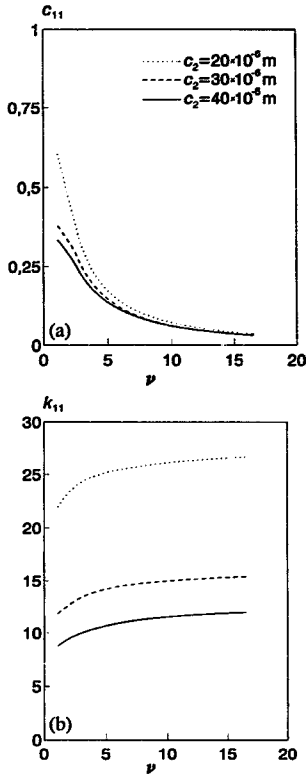


Fig. 12. (a) Damping and (b) stiffness coefficient of air ring with longitudinal rubber baffles; $n_k = 8$.

tions, we have undertaken investigations of the ring with the chamber feeding system, which is shown in Fig. 5. We have assumed that for this ring $L = 0.11$ m, $R_2 = 0.065$ m, $p_0^* = 0.7 \times 10^6$ Pa and that the feeding system consists of two rows of feedholes, eight feedholes in each row.

In the first experiment we investigated the influence of the volume V of the air chambers on the values of stiffness and damping coefficients. We have assumed that the radius of the feedholes $r_{02} = 1.0 \times 10^{-3}$ m and the orifice radius $r_d = 0.15 \times 10^{-3}$ m. The volume of the chamber is expressed by the formula:

$$V = \pi r_k^2 h_k \quad (29)$$

and as the constant value $r_k = 5.0 \times 10^{-3}$ m (radius of the chamber) is assumed, it is proportional to the chamber height h_k . Fig. 14 shows the values of C_{11} and K_{11} as a function of the frequency of vibrations ν for four different values of the chamber height $h_k = 3, 6, 9$ and 36×10^{-3} m.

While in the rings with the direct feeding system, the lower the frequency of vibration ν , the greater the values of the coefficient C_{11} were, then with the chamber feeding system there is an extremum of the function $C_{11}(\nu)$. For low values

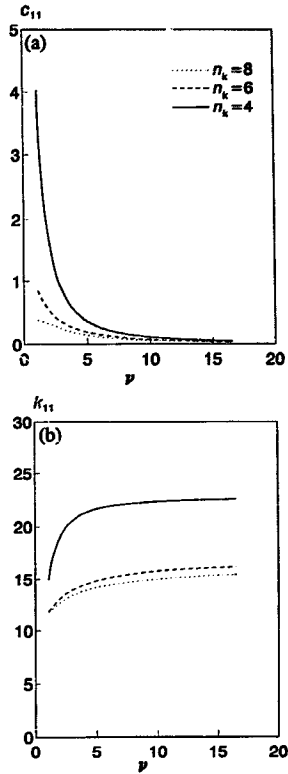


Fig. 13. (a) Damping and (b) stiffness coefficient of air ring with longitudinal rubber baffles; $c_2 = 30 \times 10^{-6}$ m.

of ν (below the extremum of C_{11}), the value of C_{11} decreases rapidly, even below zero.

It is easy to find the cause of this so far unobserved phenomenon. At sufficiently small values of the frequency ν and sufficiently small volumes ν of the chambers, significant changes of the pressure in the chambers occur during the motion of the bush. In the critical case it leads to the phenomenon of the pressure resonance described in the literature as the ‘‘pneumatic hammer’’ [23] and as a result to the loss of stability. For $h_k < 3 \times 10^{-3}$ m, this phenomenon could occur at the frequencies of free vibrations of the rotor under investigation. For sufficiently high values of ν and h_k , the motion of the bush is so fast that during one period no significant changes in the pressure p_1 in the chambers occur—the air will not ‘‘manage’’ to flow into or out of the chamber in such a quantity which would cause any significant change of the pressure. The value of the coefficient C_{11} for $\nu \approx 4\text{--}5$ lies over the boundary of the ‘‘always stable’’ loop which is approx. $C_p = 0.5$. The fact that these values of the damping coefficients are accompanied by the values of the stiffness coefficient $K_{11} = 6\text{--}8$ (for $\nu = 4\text{--}5$) is very important as it means that we are finally inside the ‘‘always stable’’ loop!

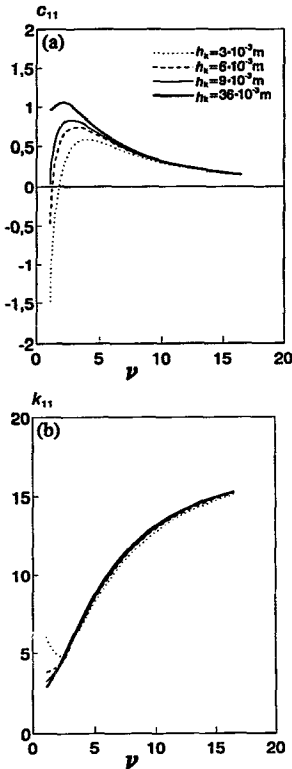


Fig. 14. (a) Damping and (b) stiffness coefficient of air ring with chamber feeding system; $r_{02} = 1.0 \times 10^{-3}$ m, $r_d = 0.15 \times 10^{-3}$ m.

Our passion of researchers has made us investigate the possibilities of influencing the values of K_{11} and C_{11} by changing other parameters of the ring, especially those of the feeding system. Fig. 15 shows how the values of these coefficients are affected by the change in the radius of the feedhole r_{02} ($r_d = 0.15 \times 10^{-3}$ m, $c_2 = 30 \times 10^{-6}$ m, $h_k = 6.0 \times 10^{-3}$ m). In this figure we also present the values of C_{11} and K_{11} of the ring with the direct feeding system transposed from Figs. 7 and 8 ($R_2 = 0.065$ m, $c_2 = 30 \times 10^{-6}$ m, $r_{02} = 0.15 \times 10^{-3}$ m) marked as the thin dotted line. As can be seen, starting from $r_{02} = r_d = 0.15 \times 10^{-3}$ m the damping coefficient increases as the radius of the feedhole increases (except for the “pneumatic hammer” region). We think that the reason for this phenomenon is the fact that while for the ring with the direct feeding system the air of the same pressure $p_0 = 7$ left each feedhole, then in the case of the ring with the chamber feeding system, pressure in each chamber on the circumference is different. Fig. 16 presents distributions of the pressure p_1 in the air chambers of the ring under investigation, for different values of r_{02} in the static equilibrium position. The force F_2 loading the ring causes a displacement of the bush in the direction of chamber 1. When the feedhole

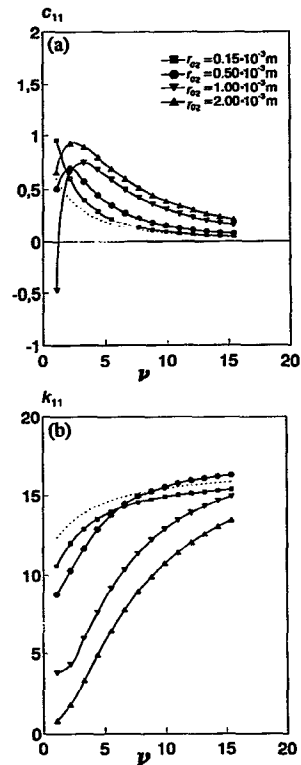


Fig. 15. (a) Damping and (b) stiffness coefficient of air ring with chamber feeding system; $h_k = 6.0 \times 10^{-3}$ m, $r_d = 0.15 \times 10^{-3}$ m.

No. 1 is covered by the bush, then the air stream \dot{m}_k coming from this chamber is the least. Hence, the pressure p_1 in this chamber is the highest. The opposite situation takes place in the case of chamber 5: the bush is at a maximum distance from it, which causes the value of the air stream coming from this chamber to be the highest, and consequently the pressure p_1 is the lowest. For $r_{02} = 0.15 \times 10^{-3}$ m the values of the pressure in the chambers are closest to the value of the supply pressure $p_0 = 7$. As the r_{02} increases, the pressures in the

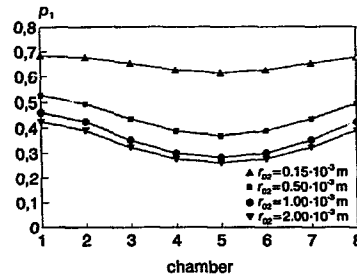


Fig. 16. Static distribution of pressure p_1 in chambers; $r_d = 10^{-3}$ m.

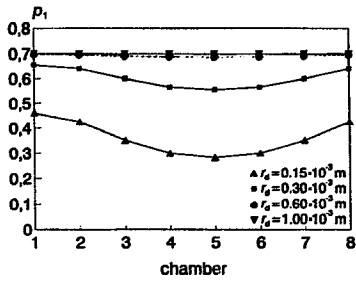


Fig. 17. Static distribution of pressure p_1 in chambers; $r_{02} = 1.0 \times 10^{-3}$ m.

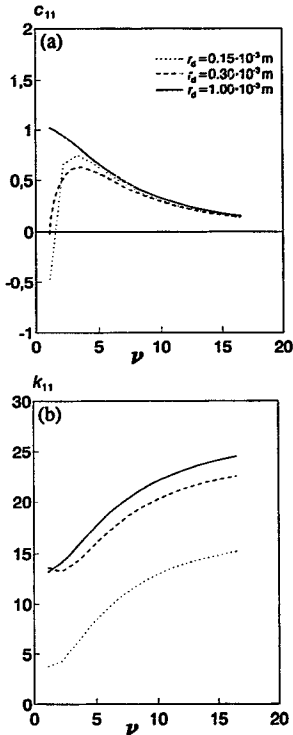


Fig. 18. (a) Damping and (b) stiffness coefficient of air ring with chamber feeding system; $h_k = 6.0 \times 10^{-3}$ m, $r_{02} = 1.0 \times 10^{-3}$ m.

chamber decrease, and the differences between them become greater and greater. This phenomenon is followed, as we have already mentioned, by an advantageous increase in the value of the damping coefficient C_{11} and an advantageous decrease in the stiffness coefficient K_{11} . For $r_{02} = 2.0 \times 10^{-3}$ m and $\nu \approx 4-5$, we observe (Fig. 15) $C_{11} \approx 0.9$ and $K_{11} \approx 4$ —such values of C_{11} and K_{11} ensure a static operation of the rotor supported in both the externally pressurised bearings as well as in self-acting bearings.

Another parameter of the feeding system that affects the coefficients C_{11} and K_{11} is the radius r_d of the orifice through

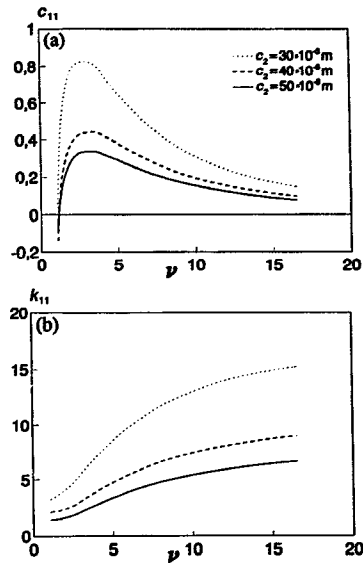


Fig. 19. (a) Damping and (b) stiffness coefficient of air ring with chamber feeding system; $h_k = 9.0 \times 10^{-3}$ m, $r_{02} = 1.0 \times 10^{-3}$ m, $r_d = 0.15 \times 10^{-3}$ m.

which the air enters the chamber. Fig. 17 shows the distribution of the pressure p_1 in the chambers (as in Fig. 16) for the ring with $r_{02} = 1.0 \times 10^{-3}$ m, $h_k = 6.0 \times 10^{-3}$ m and $c_2 = 30.0 \times 10^{-6}$ m and with the orifice radii $r_d = 0.15, 0.30, 0.60$ and 1.0×10^{-3} m. As can be seen, when the orifice radius r_d increases, aiming for the value r_{02} , the pressures in the chambers aim for the value of the supply pressure $p_0 = 7$, which is obvious. The effect of this phenomenon can be seen in Fig. 18, where the coefficients C_{11} and K_{11} are shown. For $r_d = r_{02} = 1.0 \times 10^{-3}$ m, the ring has the same damping and stiffness coefficients as the ring with the direct feeding system and $r_{02} = 1.0 \times 10^{-3}$ m. A decrease in the value of r_d causes a decrease in the value of the damping coefficient, especially in the region of the “pneumatic hammer” and near it, but these changes are small. What matters is that the decrease in the radius r_d brings about a significant (advantageous!) decrease of the damping coefficient K_{11} and “introduces” us inside the “always stable” loop.

The last parameter whose influence on stiffness and damping coefficients we investigated was the radial clearance c_2 . The results of the investigations carried out for the ring of $r_d = 0.15 \times 10^{-3}$ m, $r_{02} = 1.0 \times 10^{-3}$ m, $h_k = 9.0 \times 10^{-3}$ m and $c_2 = 30, 40$ and 50×10^{-6} m are to be found in Fig. 19. The analysis of the results is very simple: the increase in the radial clearance brings about the decrease in both the damping coefficient (which is disadvantageous) and the stiffness coefficient (which, in turn, we consider advantageous). For the system: rotor–bearings–air rings investigated by us, we consider the ring with the least value of the radial clearance $c_2 = 30 \times 10^{-6}$ m to be the optimum one.

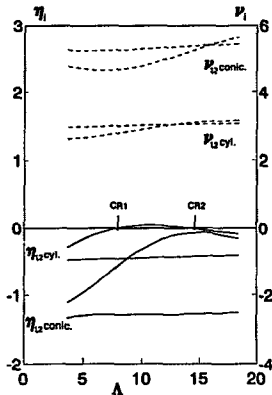


Fig. 20. Eigenvalues of the rotor with bushes supported in dampers $C_p=2$ and springs $K_p=22$.

6. Stability of the rotor supported in externally pressurised gas bearings with bushes mounted in air rings

Finally, we present the results of the investigations of the steady-state stability of the rotor whose parameters are given in Section 2 and which is supported in externally pressurised bearings.

When the bearing bushes are mounted flexibly, the system under consideration has eight degrees of freedom, hence its mathematical model (a set of differential equations of motion) has eight eigenvalues:

$$\lambda_i = \eta_i + j\nu_i \quad i = 1, \dots, 4 \quad (30)$$

The free vibrations of the system occur with the frequencies equal to the imaginary parts ν_i of the eigenvalues. As the system is symmetrical, the main modes of vibrations are cylindrical ones (the displacements of both the bearing journals are equal and are in the phase) or conical ones (the displacements of the bearing journals have the same values, but they are in the counterphase).

The signs of the real parts of the eigenvalues inform us about the stability of the static equilibrium position of the system—when the sign of the real part is positive, it means that the free vibrations of the frequency equal to the imaginary part of this eigenvalue have been self-excited.

When the rotational velocity Λ of the rotor is small enough, then the real parts of all eigenvalues are negative. If a certain value of the Λ_{CR1} is exceeded, the sign of one of the real parts of eigenvalues to which (in our rotor) the vibrations with cylindrical modes correspond changes into a positive one—a loss of the static equilibrium position and self-excited vibrations occur. If these vibrations do not destroy the bearings soon, once a further critical value Λ_{CR2} is achieved, and the self-excited vibrations vanish. The real and imaginary parts of the four basic (lowest) eigenvalues, to which the vibrations of cylindrical and conical modes correspond are shown

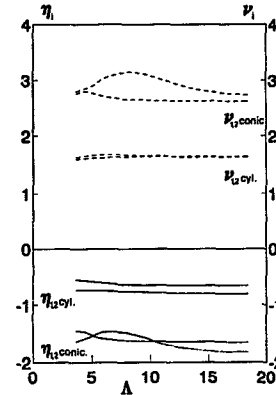


Fig. 21. Eigenvalues of the rotor with bushes supported in air ring with chamber feeding system.

in Fig. 20 for the case when a system of linear springs with $K_p=22$ and dampers with $C_p=2$ is introduced between the bearing bushes and the casing. The values of K_p and C_p have been chosen purposely beyond the “always stable” loop from Fig. 3. The boundaries Λ_{CR1} and Λ_{CR2} are marked in Fig. 2.

When the system of springs and dampers with such unfortunately selected parameters is replaced by air rings with a chamber feeding system, the vibrations are not self-excited. Fig. 21 shows the representations of real and imaginary parts of the basic four eigenvalues of the system, in which the bearing bushes are mounted in the rings with $L=0.11$ m, $R_2=0.065$ m, $r_d=0.15 \times 10^{-3}$ m, $r_{o2}=1.0 \times 10^{-3}$ m, $r_k=5.0 \times 10^{-3}$ m, $h_k=36.0 \times 10^{-3}$ m and $c_2=30.0 \times 10^{-6}$ m. As can be seen, in the whole investigated range of the rotational velocity Λ , the values of the real parts of all the eigenvalues are negative, which means that the static equilibrium position of the system is stable.

According to our expectations, the values of stiffness and damping coefficients C_{11} , C_{22} , K_{11} and K_{22} of the ring are inside the “always stable” loop. The change in the frequency of vibration 0 ($1.6 \leq \nu \leq 3.15$) cause the changes in the stiffness and damping coefficients in the range from 0.9 to 1.05 for C_{11} , C_{22} , and in the range from 3.5 to 5.9 for K_{11} , K_{22} . These ranges of the coefficients are marked in Fig. 3 as the black rectangle.

7. Conclusions

There is a possibility of eliminating self-excited vibrations of the rotor supported in gas bearings. It can be achieved by mounting the bearing bushes in air rings which perform a

role of an elastic support for these bushes. Air rings with a direct feeding system (the easiest one to obtain) have too high stiffness coefficients and too low damping coefficients to play a role of eliminators of self-excited vibrations. Suitable values of the stiffness and damping coefficients can be achieved with rings with a chamber feeding system. In spite of the positive result of our investigations, the fact is that we have not yet managed to design a ring with a damping coefficient higher than 1, retaining the stiffness coefficient lower than 10, which would be an ideal solution. We are sure, however, that it is possible. The construction of such a ring will be shown in our future works.

Appendix A. Nomenclature

A_d, A_k	areas of cross-sections of orifice ($_d$), feedhole ($_k$) (m^2)
B	inertial moment of rotor
B_p	inertial moment of joint bushes
C	dimensionless constant
C_d	dimensionless discharge coefficients in orifice ($_d$)
C_{ij}	damping coefficients of gas film
C_p	damping coefficient of elastic support
c	radial clearance of bearing (m)
FK_1, FK_2, FK_3	dimensionless constants
F_z	static loading of bearing
h_1, h_2	local film thickness, shaft bush, and bush casing, mh_k , height of chamber (m)
$H_1 (= h_1/c_1)$	dimensionless film thickness shaft bush
$H_2 (= h_2/c_2)$	dimensionless film thickness bush casing
K_{ij}	stiffness coefficients of bearing
K_p	stiffness coefficient of elastic support
l	a half of the distance between bearings
l_c	a half of the distance between dampers
l_k	a half of the distance between springs
L	length of bearing
m	mass of rotor
m_p	mass of joint bushes
m_r	reduced mass of the rotor
\dot{m}_d, \dot{m}_k	mass flows through orifice ($_d$), feedhole ($_k$) ($kg\ s^{-1}$)
\dot{m}_d^*, \dot{m}_k^*	critical mass flows through orifice ($_d$), feedhole ($_k$) ($kg\ s^{-1}$)
n_k	number of gas film sectors
$P (= p/p_0)$	dimensionless pressure in the gap shaft bush

p_a	atmospheric pressure ($N\ m^{-2}$)
p_0	supply pressure
p_e	effective pressure in annular orifice (Pa)
p_i	auxiliary theoretical pressure (Pa)
$Q (= P^2)$	dimensionless variable
\bar{Q}	mean value of Q
R_1	radius of bearing (m)
R_2	radius of ring (m)
R	universal gas constant ($J\ kg^{-1}\ K^{-1}$)
Re	Reynolds number
r_{01}	radius of plain feedhole of bearing (m)
r_{02}	radius of plain feedhole of air ring (m)
r_d	radius of orifice (m)
r_k	radius of chamber (m)
T_0	constant gas temperature (K)
t	time (s)
V	volume of chamber (m^3)
$\beta \left(= \left(\frac{2}{\kappa+1} \right)^{\kappa/(\kappa-1)} \right)$	critical pressure ratio
κ	isentropic expansion index
γ_r	angle of seal (rad)
Δt	increment in time (s)
σ	gas viscosity ($N\ s\ m^{-1}$)
ϵ	relative eccentricity ratio shaft bush
θ, ξ	dimensionless coordinates of gas film, related to R_1
μ	viscosity ($N\ s\ m^{-2}$)
Λ	dimensionless bearing number
λ_i	complex eigenvalues
ν	dimensionless mass flow rates
ν_d, ν_k	dimensionless mass flow through orifice ($_d$), feedhole ($_k$)
$\pi_d (= p_1/p_0)$, $\pi_e (= p_e/p_2)$, $\pi_i (= p_i/p_2)$	pressure ratios
$\tau (= \Omega t / 2M)$	dimensionless time
Ω	angular frequency of vibration ($rad\ s^{-1}$)
ω	angular velocity of shaft ($rad\ s^{-1}$)

Appendix B

All the dimensionless parameters which are used in the paper are related to the bearing parameters:

$$C_{ij}^* [N\ s\ m^{-1}] = \frac{2\Lambda p_a R^2}{\omega c} C_{ij} K_{ij}^* [N\ m^{-1}] = \frac{p_a R^2}{c} K_{ij}^*$$

$$m^* \text{ [kg]} = \frac{4\Lambda^2 p_a R^2}{\omega^2 c} m \quad B^* \text{ [kg m}^2\text{]} = \frac{4\Lambda^2 p_a R^4}{\omega^2 c} B$$

$$\omega \text{ [rad s}^{-1}\text{]} = \frac{p_a c^2}{6\sigma R^2 \Lambda} \quad \nu^* \text{ [rad s}^{-1}\text{]} = \frac{\omega}{2\Lambda} \nu \quad t \text{ [s]} = \frac{2\Lambda}{\omega} \tau$$

$$l^* \text{ [m]} = Rl \quad F^* = \frac{1}{p_a R^2} F$$

References

- [1] J.W. Lund, The stability of an elastic rotor in journal bearings with flexible, damped supports. *Trans. ASME, J. Appl. Mech. Ser. A*, (1965) 911–920.
- [2] J. Kerr, The Onset and cessation of half-speed whirl in air-lubricated self-pressurized journal bearings. *NEL Report No. 273*, Glasgow, 1966.
- [3] Z. Kazimierski and K. Jarzecki, Stability threshold of flexibly supported hybrid gas journal bearings. *Trans. ASME, J. Lubr. Technol., Ser. F*, 101 (1979) 451–457.
- [4] H. Marsh, The stability of self-acting gas journal bearing with noncircular members and additional elements of flexibility. *Trans. ASME, J. Lubr. Technol., Ser. F*, (1969) 113–119.
- [5] K. Czolczyński, Stability of flexibly mounted self-acting gas journal bearings, *Nonlinear Science B*, Vol. 7, Chaos and Nonlinear Mechanics, World Scientific, Singapore, 1994, pp. 286–299.
- [6] K. Czolczyński, Stability of flexibly mounted, self-acting gas journal bearings, *XVI Symposium Vibrations in Physical Systems*, Białeżewko, Poland, 1994, pp. 89–90 (summary).
- [7] K. Czolczyński, Stateczność i drgania samowzbudne wirnika podpartego w łożyskach gazowych (Stability and self-excited vibrations of a rotor supported in gas bearings), *Zesz. Nauk. PE*, (1994) 6942–132 (in Polish)
- [8] K. Czolczyński and K. Marynowski, Stability of symmetrical rotor supported in flexibly mounted, self-acting gas journal bearings, *Wear*, in press
- [9] K. Czolczyński and K. Marynowski, How to avoid self-excited vibrations in symmetrical rotors supported in gas journal bearings, *Machine Dyn. Problems*, in press.
- [10] K. Czolczyński and K. Marynowski, Stability of unsymmetrical rotor supported in gas journal bearings, *Machine Vibration*, in press.
- [11] K. Czolczyński, Hopf bifurcation in gas journal bearings. *Trans ASME Appl. Mech. Rev.* (1993) 46392–398.
- [12] V. Castelli and H.G. Elrod, Solution of the stability problem of 360 degree self-acting gas-lubricated bearings, *Trans. ASME, J. Basic Eng. Ser. D*, 87(2) (1965) 199–212.
- [13] L., Brzeski and Z., Kazimierski, High stiffness bearing, *ASME, J. Lubr. Technol.*, 101 (1979) 520–525.
- [14] Z. Kazimierski and J. TrojnarSKI, Investigations of externally pressurized gas bearings with different feeding systems, *ASME, J. Lubr. Technol.*, 102 (1980) 59–64.
- [15] H.G. Elrod and G.A. Gianfield, Computer procedures for the design of flexibly mounted, externally pressurized, gas lubricated bearings, *Proc. Gas Bearing Symp.*, University of Southampton, 1971, Paper 22.
- [16] Z. Kazimierski and J. Krysiński, *Łożyskowanie gazowe i napędy mikroturbinowe*, WNT, Warszawa, 1981 (in Polish).
- [17] K., Czolczyński, L. Brzeski and Z. Kazimierski, High stiffness gas journal bearing under the step force, *Wear*, 167 (1993) 49–58.
- [18] K. Czolczyński, Stability of high stiffness gas journal bearing, *Wear*, 172 (1994) 175–183.
- [19] K. Czolczyński, High stiffness gas journal bearings in grinding machines, *Machine Dyn. Problems*, 5 (1993) 65–87.
- [20] L. Brzeski and Z. Kazimierski, Infinite stiffness gas bearings for precision spindles, *Precision Eng.*, 14(2) (1992) 105–109.
- [21] S.P. Carfagno and J.T. McCabe, Summary of Investigations of Entrance Effects in Circular Thrust Bearing, Franklin Inst. Lab. for Res., Philadelphia, PA, *Interim Report I-2049-24*.
- [22] E. Dudgeon and H.I.R.G. Lowe, National Research Council of Canada, Ottawa, Ont., *Report MT-54*, 1965.
- [23] H. Mori and A. Mori, On the stabilizing methods of externally pressurized thrust gas bearings, *Trans. ASME, J. Lubr. Technol., Ser. F*, (1967) 283–290.

Biographies

Krzysztof Czolczyński was born in 1956. He is Senior Lecturer in the Division of Dynamics, Technical University of Łódź, Poland. He received a Master of Science in Applied Mechanics (1980), Ph.D. (1988) and Doctor of Science (1994) from the Technical University of Łódź. He has fifteen years of scientific experience in vibration analysis, rotor dynamics, theory of machines and mechanisms and first of all in dynamics of gas bearings. He has a number of publications in the area of rotor dynamics and gas bearings.

Tomasz Kapitaniak was born in 1959. He is the Chief of Division of Dynamics, Technical University of Łódź, Poland. He received a Master of Science in Mechanical Engineering (1982), PhD (1985) and Doctor of Science (1988) from the Technical University of Łódź. He is Professor since 1991. He has fourteen years of scientific experience in vibration analysis, chaos and automatic control. He has many publications in the area of chaotic motion of mechanical systems.

Krzysztof Marynowski was born in 1950. He is Senior Lecturer in Division of Dynamics, Technical University of Łódź, Poland. He received a Master of Science in Applied Mechanics (1975) and Ph.D. (1983), from the Technical University of Łódź. He has twenty years of scientific experience in vibration analysis, rotor dynamics and automatic control. He has several publications in the area of rotor dynamics.